Time-resolved infrared transmittance and reflectance of a propagating melt in GaAs

Brian J. Keay, Marcus Mendenhall, and Glenn S. Edwards
Department of Physics and Astronomy and the W.M. Keck Free-Electron Laser Center, Vanderbilt University, Nashville, Tennessee 37235
(Received 23 July 1999)

The time-resolved infrared transmittance and reflectance of a melt induced by a 10 nsec optical-laser pulse has been observed in an undoped crystalline GaAs wafer. Picosecond pulsed, 2.86 GHz repetition rate, infrared radiation from a free-electron laser was used to study the formation and propagation of the melt in real time. The back reflectance (probed from the side opposite to the incident optical radiation) displays interference oscillations as the melt propagates in the sample. The measurements are in agreement with model calculations which describe the melt with the Drude free-carrier model. [S0163-1829(99)01440-X]

The study of laser-induced phase transitions in semiconductors has been a topic of considerable interest for both the basic physics and for the materials engineering applications. The physics of the laser-induced phase transition is believed to be strongly dependent on the intensity and time duration of the pump pulse.[1–3] The important time scale is associated with the time it takes for the electron-hole plasma excited by the optical laser to transfer its energy to the lattice via longitudinal optical phonon emission, which is about 2 psec in the case of GaAs.[4] Experiments which have used femtosecond pulses to observe melting before the carriers have had time to relax[2,3] observe a direct electronic melting process for which thermal melting models are not relevant. Alternatively, if the melting process requires more than a few picoseconds to commence, it has been established, after some controversy, that the melting process is well described by thermal melting models.[5–8] Several laser melting studies have also shown[9–11] that the frequency dependence of the dielectric function of molten silicon and germanium are consistent with the Drude free-carrier model. The dielectric properties of molten GaAs, however, have been more difficult to determine. One of the challenges in studying the optical properties of molten GaAs has been its tendency to form a gallium-rich surface due to rapid arsenic evaporation.[8,12,13] Early experiments using IR radiation at 1.064 μm and 1.9 μm observed that the front reflectivity of molten GaAs increases with increasing probe frequency,[14] which is the opposite behavior one would expect if the Drude free-carrier model were applicable. More recent work has focused on measuring the dielectric function of GaAs on ultrafast time scales using photon energies that are greater than the band-gap energy.[3] Relatively few studies of molten GaAs have used infrared probes.

In the work discussed here, infrared radiation provided by Vanderbilt's Mark III free-electron laser (FEL) (Ref. 15) was used to perform time-resolved transmittance and reflectance measurements on both sides of an undoped 400 μm thick (100) GaAs wafer simultaneously. The picosecond pulsed, 2.86 GHz repetition rate IR radiation from the FEL allows the formation and propagation of the melt to be monitored on thermal time scales. The propagating melt produces a destructive interference pattern which can be used to determine the melt thickness and velocity. The use of an infrared back probe also enables a reflectance measurement of the liquid-solid interface as it propagates deep into the sample (compared to the relevant skin depths). This fact becomes particularly useful for pump fluences intense enough that explosive vaporization of surface material renders front probes inadequate. For these intense pump pulses, the back reflectance forms a plateau which can last several hundred nanoseconds. The dependence of the plateau's height on the FEL wavelength appears to be consistent with the Drude free-carrier model.

The IR probe measurement used a single FEL macropulse, i.e., a 3–5 μsec train of about 10 000 *micropulses*. Each micropulse has a full width at half maximum (FWHM) of 1 psec and the separation between the micropulses is 350 psec.[15] This provides a 2.86 GHz micropulse repetition rate which reduces considerably the amount of heating of the melt by the probe while enabling the motion of the liquid-solid interface to be monitored in real time. The optical radiation is provided by a Nd:YAG (yttrium aluminum garnet) laser frequency doubled to a wavelength of 532 nm, which is incident 4.5° to the surface normal and focused to a 4.3 mm diameter spot size. The FWHM of the optical pulse is 10 nsec, but the pulse is not Gaussian in time or space. The pulse consists of many optical modes designed to give a ''flat-top'' spatial profile. Timing electronics synchronize and center the 10 nsec Nd:YAG pulse inside one 3–5 μsec FEL *macropulse*. Beam splitters are used to split each *s*-polarized FEL pulse into a reference pulse and two probe pulses which were focused to a 200 μm diameter spot size. The back-probe pulse was incident on the side of the sample opposite to the optical pump pulse and 16° to the surface normal (Fig. 1). This pulse was used to measure the transmittance (T) as well as the back reflectance (R_b). The second probe pulse was used to measure the front reflectance (R_f) and was incident on the same side as the pump pulse and 40° to the surface normal. The FEL macropulse energy is kept below 15 μJ, yielding an average micropulse fluence of less than 6 μJ/cm^2. Each set of transmission/reflection curves requires only one pump pulse and one probe macropulse. The sample was translated after every optical pulse to ensure that data were taken only on fresh material. Four photoelectromagnetic detectors (Boston Electronics PEM-L-3) with 0.2 nsec response times were used to simultaneously mea-

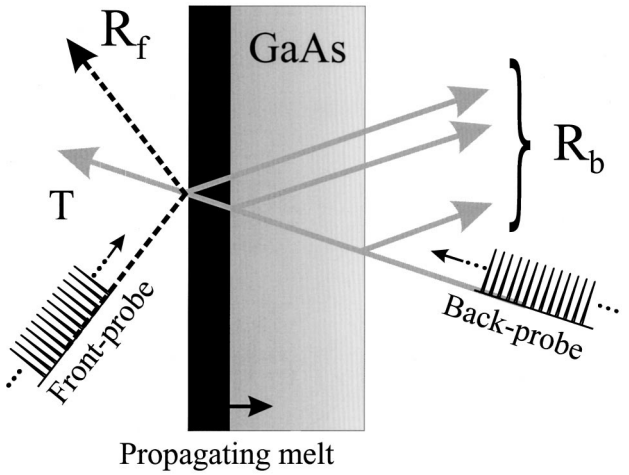

FIG. 1. Schematic of the experimental setup. The sample is pumped on the front surface with the 10 nsec optical-laser pulse (not shown) and the transmittance T, front reflectance R_f, and back reflectance R_b are probed with the train of infrared micropulses from the FEL. The black region represents the propagating melt and, for clarity, is not to scale.

sure T, R_f, R_b, and a reference pulse used for normalization. The traces were recorded using a Hewlett-Packard four channel oscilloscope (HP 54845A Infinium) which has less than a 700 psec response time for each channel. The experiment was performed both with and without collection optics, with the same results.

The left column in Fig. 2 shows a typical set of measurements for T, R_f, R_b, and the absorbance ($A=1-R_b-T$) at a FEL wavelength of 7.7 μm. In Fig. 2(a), the optical-pulse fluence is below the calculated melting threshold ($\Phi=0.21$ J/cm^2). Both R_b and R_f display a decrease induced by the 10 nsec optical pulse which strikes the sample at $t\approx 0$. At this energy level it is unlikely that much melting has occurred; the decrease in R_f and R_b can be attributed to a free-carrier plasma whose plasma frequency is less than the probe frequency (2.5×10^{14} Hz). This can be understood from the Drude contribution to the dielectric function,

$$\epsilon(\omega)=\epsilon_m\left(1-\frac{\omega_p^2}{\omega(\omega-i/\tau)}\right), \tag{1}$$

where τ is the relaxation time and ϵ_m is the crystalline dielectric constant at the GaAs melting temperature (1511 K). The plasma frequency is given by $\omega_p=\sqrt{n_e e^2/\epsilon_m\epsilon_0 m}$ and n_e is the charge density. From the Drude free-carrier model one would expect to observe a dramatic increase in the reflectance once melting has been induced. This is verified in Fig. 2(c) for a pump pulse just above the melting threshold. Both R_f and R_b decrease immediately after excitation, corresponding to a plasma frequency ω_p which is less than the probe frequency ω. Once melting has occurred, the plasma frequency jumps from a value that is less than the probe frequency to a value that is greater than the probe frequency. After the initial decrease, a sudden increase in R_f is observed at $t\approx 10$ nsec. The rapid increase in R_f signals the onset of melting and the formation of the highly reflective molten surface layer which expands into the sample. This is followed by a monotonic decrease to the initial value of the

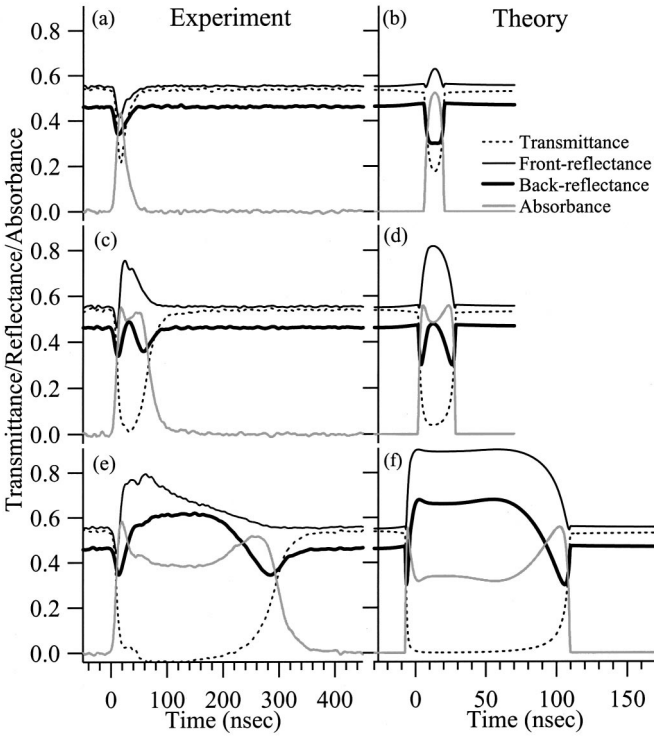

FIG. 2. The measured (left column) and calculated (right column) T (dotted line), R_f (thin black line), R_b (thick black line), and absorbance A (gray line) at a FEL wavelength of 7.7 μm for different optical-pump fluences, Φ. Subthreshold for melting: measured (a) and calculated (b) $\Phi=0.204$ J/cm^2. Just above the melting threshold: measured (c) $\Phi=0.29\pm 0.04$ J/cm^2 and calculated (d) $\Phi=0.24$ J/cm^2. Well above the melting threshold: measured (e) $\Phi=0.85\pm 0.22$ J/cm^2 and calculated (f) at $\Phi=0.5$ J/cm^2.

reflectance as the sample cools and the melt front recedes back to the surface. The back reflectance R_b in Fig. 2(c) displays an unusual oscillatory behavior, two minima separated by a local maximum. Unlike the front reflectance, however, whether this local maximum reaches or surpasses the initial, unpumped value of R_b depends on how far the melt propagates into the sample. Furthermore, as the sample begins to cool, the back reflectance goes through a second minimum at $t\approx 58$ nsec before increasing monotonically to the initial, unpumped value of R_b. Finally, for an optical-pump fluence substantially above the melting threshold [Fig. 2(e)] we see that R_b reaches a maximum and forms a plateau that can last for several hundred nanoseconds.

To develop a more detailed understanding of the measurements shown in Fig. 2, we used a thermal melting model[6–8] to calculate the temperature as a function of distance into the sample and as a function of time. A Gaussian pulse with a FWHM of 10 nsec that reaches its peak power on the sample surface at $t=0$ drives the heating process. The calculated temperature profiles are then used as input for a calculation of the time evolution of the optical properties using a standard multilayer matrix approach.[16] A 14–20 μm surface region is divided into ≈ 5000 layers and the dielectric function of the ith layer was taken to be $\epsilon_i=\epsilon(\omega)\hat{L}_i+\epsilon(T_i)(1-\hat{L}_i)$, where $\epsilon(T_i)=\epsilon_\infty[(1-9.0)\times 10^{-5}T_i]$ is the dielectric function of a crystalline layer at a temperature less than 1511 K.[17] $\hat{L}_i=L_i/L_m$ is the ratio of latent heat absorbed by the ith layer

to the latent heat of melting. $\hat{L}_i$ is a parameter for the melting transition of the ith layer and is 0 for no melting and 1 for complete melting. An important assumption in the model is that the dielectric function of a layer that has completed the melting process, $\epsilon(\omega)$, can be described by the Drude free-carrier response in Eq. (1). The values of n_e and τ are obtained from dc conductivity measurements of molten GaAs; these are 1.9×10^{23} cm^{-3} and 1.5×10^{-16} sec, respectively.[14,18]

The results of the calculation are shown in the right column of Fig. 2 for three different fluence levels. At a fluence level of $\Phi=0.204$ J/cm^2 [Fig. 2(b)], no single layer completes the melting process. At $t\approx19$ nsec, the fraction of latent heat of melting absorbed by the surface layer ($i=0$) reached $\hat{L}_i=0.90$, the closest the sample came to melting. It should be noted that the calculated R_f shown in Fig. 2(b) actually increases as a result of the optical pump pulse, in contradiction with the experimental result shown in Fig. 2(a). This is because the calculations only take into account changes in the dielectric function as a result of melting and not the initially excited charge carriers which act to reduce the real part of the dielectric constant. The comparison between Figs. 2(a) and 2(b) suggests that even when the sample comes very close to melting (i.e., $\hat{L}_i=0.90$), it is still in the crystalline state. The thermal model presented here gives a more accurate description of the optical processes once melting has been induced. This can be seen in Figs. 2(d) and 2(f). Figure 2(d) reproduces the oscillations in the back reflectivity observed in the experiment [Fig. 2(c)].

It is interesting to note that the amount of radiation reflected from the back *surface* of the sample is not affected by the pump pulse and remains constant throughout the measurement (see Fig. 1). The initial, unpumped value of R_b is 0.46. This consists of the constant contribution from the back surface, 0.30, and an additional 0.16 from multiple reflections inside the sample. Initially, the multiple reflections only occur between the front and back surface of the sample. When the melt forms, the back reflectance begins to decrease due to destructive interference and absorption. The melt layer both absorbs radiation and provides a Fabry-Perot-like cavity. The minima in R_b occur when the melt thickness reaches ≈8 nm, which is much less than a quarter wavelength $\lambda/4(142$ nm), as well as the optical skin depth (≈45 nm). Nevertheless, the contribution to R_b from multiple reflections drops from 0.16 to zero at this thickness. No IR radiation is reflected by the melt at the minima, but radiation is still transmitted. The reflective properties of the molten layer in this model are independent of wavelength when the melt thickness is less than the skin depth. The results shown in Figs. 2(c) and 2(d), for example, are independent of IR wavelength. The maximum melt thickness of 37 nm was reached at $t\approx13$ nsec in Fig. 2(d).

When the melt thickness propagates beyond the skin depth of the IR radiation, very little of the back-probe radiation reaches the front surface of the sample and destructive interference starts to have a negligible effect. As this occurs, R_b reaches a maximum that can last several hundred nanoseconds [Figs. 2(e), 2(f), and 3]. The back-reflectance maxima obtained from the average value on the plateaus have a wavelength dependence consistent with the Drude free-carrier model, as shown in Fig. 3. Figure 3(a) shows the measured R_b at 2.7, 6.45, and 7.7 μm compared to the calculation in Fig. 3(b). The qualitative agreement between the theory and experiment is quite good, but there are a couple of notable discrepancies. First, the time scales in the calculation at low pump fluences appear to be too short compared to the experiment. The average time between the minima in R_b for three data sets similar the one in Fig. 2(c) is 39 ± 6 nsec, compared to 21.5 nsec in the calculation [Fig. 2(d)]. Some of this discrepancy may be explained by the fact that significant arsenic evaporation begins to occur at ≈900 K (Refs. 5,8,12, and 13) and results in the formation of a thin gallium residue on the sample surface. Arsenic evaporation, the ejection of material, and the charge carriers excited directly by the optical laser were not included in the optical part of the calculation. What is perhaps more important, however, is that the ''flat-top'' spatial profile of the Nd:YAG laser does not provide ideal, uniform illumination. Thirteen data sets whose time between the two back-reflectance minima, $\delta t_{\min}$, fell in the range 225–323 nsec were averaged to obtain 280 ± 22 nsec. These data sets had an average pump fluence of 0.85 ± 0.22 J/cm^2. For comparison, at a YAG fluence of 0.85 J/cm^2 the calculation gives 299.5 nsec between the reflectance minima shown in Fig. 3(b). The large standard deviations in the measured fluence are due to large fluctuations in the spatial profile of the YAG pulse, which were clearly visible using a two-dimensional detector array. The spatial nonuniformities in the YAG pulse fluence will result in thickness nonuniformities which could also explain some of the broadening around the reflectance minima observed in the experiment and the fact that the multiple reflections are not completely suppressed at the back-reflectance minima. If the multiple reflections were completely suppressed, the value of the minima in R_b would be 0.30 (see Fig. 3). The reflectance maxima obtained from the experiment also appear to be damped by melt thickness nonuniformities, as can be seen in Figs. 3 and 4. The maximum

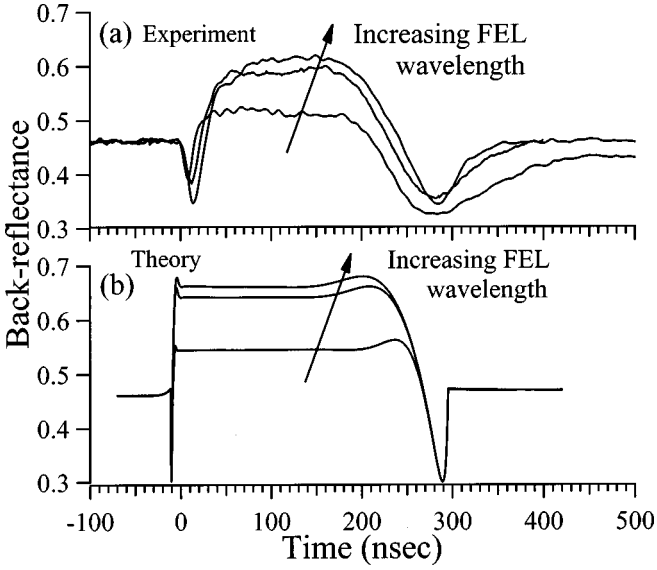

FIG. 3. The measured (a) and calculated (b) R_b at FEL wavelengths of 2.7, 6.45, and 7.7 μm (increasing wavelength corresponds to increased reflectance). The optical-pump fluence for the calculation was $\Phi=0.85$ J/cm^2.

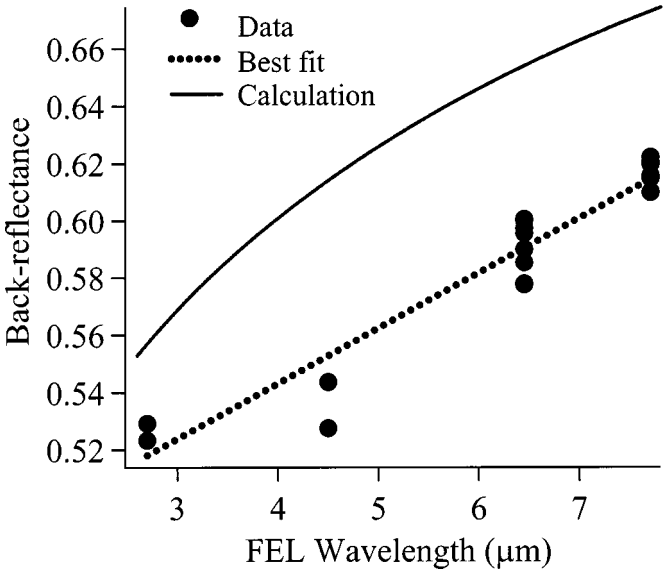

FIG. 4. The back-reflectance maximum as a function of FEL wavelength. The points are measured values of the back reflectance when a plateau is formed for several measured traces. The dotted line is the best fit to the data and the solid line is the calculation.

value of the back reflectance is plotted versus wavelength in Fig. 4 for FEL wavelengths of 2.7, 4.5, 6.45, and 7.7 μm. The solid line is the calculation and the dotted line is a fit to the data. The wavelength dependence of the back-reflectance maximum is consistent with the Drude free-carrier model, but there is a clear offset between the calculation and the data points. At a FEL wavelength of 7.7 μm, for example, the maximum in R_b obtained from the average value on the plateau is 0.62 compared to the calculated value of 0.66. The fact that the reflectance values at the maximum and the minima disagree with the calculation by roughly the same amount is consistent with melt thickness nonuniformities. In fact, for the melt to behave as a well defined reflecting surface or to observe destructive interference, it is likely that the optical radiation must have a shallow penetration depth in order to prevent the melt thickness nonuniformities from being too large. The penetration depth of 532 nm radiation in crystalline GaAs is 128 nm, compared to 820 nm in silicon. We were unable to observe similar interference patterns or a back-reflectance maximum in silicon.

The spatial fluctuations in the pump pulse would account for discrepancies in the calculated and measured melt velocities. The average resolidification velocity, for example, can be estimated from the distance the liquid-solid interface travels in the time between the trailing edge of the plateau and the second minimum in R_b shown in Fig. 3. At a FEL wavelength of 7.7 μm, the distance the melt travels in this time was determined from the calculation to be 112 nm. The corresponding resolidification velocities are 1 m/sec for the measurement [Fig. 3(a)] at a FEL wavelength of 7.7 μm and 1.5 m/sec for the calculation [Fig. 3(b)]. The rounding in the plateaus due to melt thickness nonuniformities would account for most of the difference.

It should be mentioned that the front reflectance R_f also approaches a maximum at the higher fluence levels as shown in Fig. 2(e), but no clear frequency dependence was observed. Furthermore, for only slightly higher fluences than for the data shown in Fig. 2(e), the front reflectance would actually decrease by at least 50% before recovering in several hundred nanoseconds. This is indicative of severe damage to the surface, which may include the ablation and explosive vaporization of material. The back reflectance for the higher fluence levels, however, appears relatively insensitive to the violent surface reactions.

In conclusion, picosecond pulsed, 2.86 GHz repetition rate, infrared radiation from an FEL has been used to monitor the formation and propagation of an optical-laser-induced melt on thermal time scales. The back reflectance displays a destructive interference pattern as the melt expands into the sample and again as the melt front recedes back to the surface when the sample cools. When the melt thickness expands beyond the penetration depth of the infrared radiation, a wavelength dependence of the back reflectance is revealed. This wavelength dependence is consistent with the Drude free-carrier model. The results discussed here suggest a method of monitoring the effects of laser annealing of buried layers as the melt expands deep into a sample and then recedes to the surface, analogous to methods used to study amorphous silicon.[19]

We would like to thank the staff of the W. M. Keck Free-Electron Laser Center. This research was supported by the DoD MFEL Program under Contract No. ONR N00014-94-1023.

[1] K. Sokolowski-Tinten, H. Schulz, J. Bialkowski, and D. von der Linde, Appl. Phys. A: Solids Surf. **53**, 227 (1991).

[2] P. Saeta, J.-K. Wang, Y. Siegal, N. Bloembergen, and E. Mazur, Phys. Rev. Lett. **67**, 1023 (1991).

[3] Li Huang, J.P. Callan, E.N. Glezer, and E. Mazur, Phys. Rev. Lett. **80**, 185 (1998); E.N. Glezer *et al.*, Phys. Rev. B **51**, 9589 (1995); **51**, 6959 (1995).

[4] J.A. Kash *et al.*, Phys. Rev. Lett. **54**, 2151 (1985).

[5] D.H. Lowndes and R.F. Wood, Appl. Phys. Lett. **38**, 971 (1981).

[6] *Pulsed Laser Processing of Semiconductors*, Semiconductors and Semimetals Vol. 23, edited by R.F. Wood, C.W. White, and R.T. Young (Academic, Orlando, 1984).

[7] R.F. Wood and G.E. Jellison, Jr., Ref. 6, p. 166; R.F. Wood and G.E. Giles, Phys. Rev. B **23**, 2923 (1981); R.F. Wood *et al.*, *ibid.* **53**, 15 863 (1996).

[8] Z.L. Wang and F.W. Saris, Phys. Lett. **83A**, 367 (1981).

[9] C.V. Shank, R. Yen, and C. Hirlimann, Phys. Rev. Lett. **50**, 454 (1983); *ibid.* **51**, 900 (1983).

[10] J.M. Liu, H. Kurz, and N. Bloembergen, in *Laser-Solid Interactions and Transient Thermal Processing of Materials*, edited by J. Narayan, W. L. Brown, and R. A. Lemons, Vol. 13 of Materials Research Society Symposia Proceedings (MRS, Pittsburgh, 1983), p. 3.

[11] G.E. Jellison, Jr. and D.H. Lowndes, Appl. Phys. Lett. **51**, 352 (1987).

[12] R. Tsu *et al.*, Appl. Phys. Lett. **34**, 153 (1979).

[13] See D. H. Lowndes, in Ref. 6, p. 505.
[14] J.M. Liu, A.M. Malvezzi, and N. Bloembergen, Appl. Phys. Lett. **49**, 622 (1986).
[15] G.S. Edwards *et al.*, IEEE J. Sel. Top. Quantum Electron. **2**, 810 (1996).
[16] T. E. Jenkins, *Semiconductor Science: Growth and Characterization Techniques* (Prentice Hall, UK, 1995), p. 250.
[17] J.S. Blakemore, J. Appl. Phys. **53**, R123 (1982).
[18] V. M. Glazov, S. N. Chizhevskaya, and N. N. Glazoleva, *Liquid Semiconductors* (Plenum, New York, 1969).
[19] D.H. Lowndes *et al.*, Appl. Phys. Lett. **48**, 1389 (1986).